J Porous Mater (2006) 13: 21–26
DOI 10.1007/s10934-006-5486-2

# Dynamic Young's modulus of open-porosity titanium measured by the electromagnetic acoustic resonance method

**Chengfeng Li · Zhengang Zhu**

Received: February 10, 2005 / Revised: August 2, 2005


**Abstract** As biological implants, porous titanium with adjustable mechanical properties can solve the stress-shielding effect. In this paper, porous titanium was prepared by the powder metallurgy method, where urea powders as the second phase were removed by heat treatment. Pore morphology (such as pore size and character) was controlled by the character of urea powders. The dynamic Young's moduli of such porous titanium with different morphology was measured by the electromagnetic acoustic resonance method. From the semi-log plots of Young's modulus versus the porosity, it was found that with increased porosity this modulus firstly decreases linearly, then decreases rapidly and goes to zero at certain porosity. However, the Young's modulus was independent of pore size. The relationship between Young's modulus and the porosity was explained by a parallel model based on the Minimum Solid Area method. The value of linear slop '$b$' and the percolation limit '$P_C$' were used for predicting the trend of Young's modulus varied with the porosity and pore size. So porous titanium with appropriate Young's modulus can be chosen as a candidate for bone substitutes.

**Keywords** Porous titanium · Powder metallurgy · Dynamic Young's modulus · Bone implant · Minimum Solid Area method

C. Li (✉) · Z. Zhu
Key Laboratory of Materials Physics, Institute of Solid State Physics, Chinese Academy of Sciences, Hefei, Anhui, 230031, P. R. China
e-mail: cfli@issp.ac.cn

## 1. Introduction

Titanium is welcome as biological implants, because of its high corrosion resistance and good biocompatibility [1]. But great mechanical mismatch between solid titanium and bones will cause stress-shielding effect [2, 3], which retards its use as bone substitute. If pores are introduced, the mechanical properties of porous titanium can be adjusted by its porosity [4, 5]. Porous titanium with the porosity in a wide range is prepared by the powder metallurgy method [6], where pores are generated after fugitive space-holders as the second phase are removed during heat treatment. Many kinds of powders are selected as space-holders, for example, stearin [7], urea [8], ammonium hydrogen carbonate [9, 10], polymer granules [11], etc.

Before applying porous titanium in surgery, the relation between mechanical properties and pore morphology must be clarified. Young's modulus is an important parameter describing the mechanical properties of materials. For porous solids, pore always acts as an internal notch [12] and the tensile stress-strain curve is schematically shown in Fig. 1 [13, 14], where $E_1$ and $E_2$ are called dynamic Young's modulus and apparent Young' modulus, respectively. The deviation at Point N is due to the localized yielding at the pores. Using tensile testing the dynamic Young' modulus $E_1$ is difficult to determined and if the deviation from linearity starts very early, the modulus $E_2$ is actually measured. Ultrasonic or sonic measurement is used to measure $E_1$, due to the small strain caused in the sample [15–17]. In this paper, firstly porous titanium with different pore morphology was prepared by the powder metallurgy method and then the dynamic Young's modulus of such porous titanium was measured by the electromagnetic acoustic resonance (EMAR) method [18]. The relationship

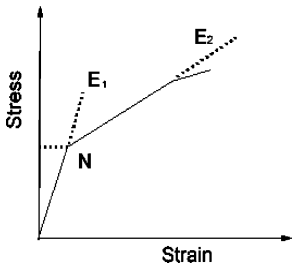


**Fig. 1** Schematic diagram of the tensile stress-strain curve for a notched sample

between dynamic Young's modulus and their morphology was also studied in detail.

## 2. Experiments

### 2.1. Preparation of samples

Commercial pure Titanium (−300 mesh, purity >98.6%) was used. Urea powders (analytical pure) were selected as space-holders and machined to different size: −80 + 100 mesh (series A), and +60 mesh (series B). After titanium and urea powders were well mixed, the mixture was compacted in a stainless-steel die. The pressure increased slowly to 150 MPa for powders arranged and settled and held for one minute to gain green bodies with saturated distributions of densities. The procedure of heat treatment in a flow of ultra pure argon air was performed in two steps: the first was heating at 200°C for 2 h to remove urea powders and the second was at 1200°C for 4 h to densify the body. Through changing the weight ratio of titanium to urea powders, samples with different porosity were gained. While urea powders of series A or B were used, samples with different pore size were prepared. The size of all samples was cut to 1.5–3.0 mm × 3.0 mm × 70 mm by an electrosparking machine. The microstructure of porous titanium after polished on the diamond paste with grits size descending from 50 $\mu$m to final polishing at 5 $\mu$m was characterized by Scanning Electric Morphology (SEM).

### 2.2. Test of Dynamic Young's modulus

In the EMAR method, the sample is excitated to flexural vibrations by the Lorentz force from the alternating signals. There will be resonance frequency spectroscopy while varying excitated signals [19]. If hanging the sample on the nodal points at the distance from the free end of 0.224$l$ and 0.776$l$ where $l$ is the whole length, the fundamental resonance mode was measured with the frequency named $f_r$ [20]. On the base of the motion of the flexural vibration, the dynamic Young's modulus ($E$) is calculated from the formula [21] as:

$$E = 0.94646 \times \left(\frac{l}{a}\right)^3 \times f_r^2 \times \left(\frac{W}{b}\right) \times T \times 10^{-6}\ (\mathrm{N/mm^2}) \quad (1)$$

where $a$, $b$ and $W$ is the thickness, width and weight of the sample, respectively. In Eq. (1), 'T' is a correction factor and taken as '1'.

## 3. Results and discussion

### 3.1. Morphological characterizations

The apparent density is calculated as the weight of a sample over the volume. The porosity is one minus the relative density. The pore size is determined as the average of sizes of 10 pores. Microstructures of samples with different porosity and pore size are characterized by SEM and shown in Fig. 2.

While mixing, urea powders are always covered by titanium powders forming composed cells named Cell A as simplified in Fig. 3(A). During compacting in the die, ductile

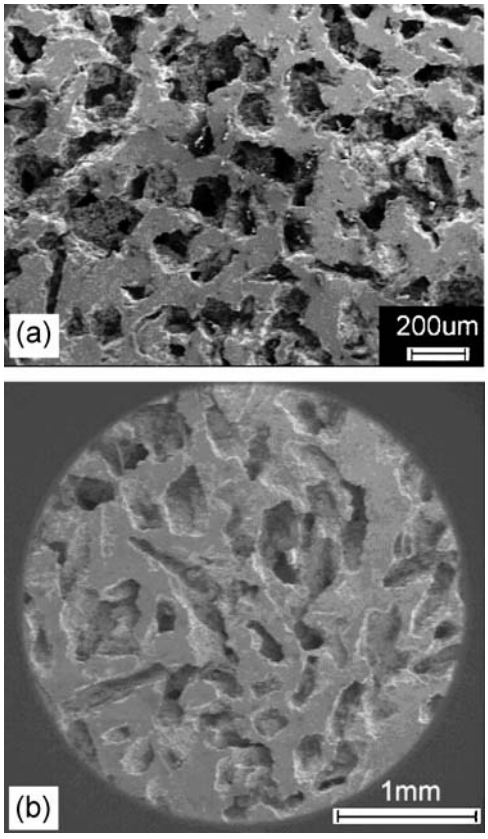


**Fig. 2** SEM imagine of the porous titanium. (a) Sample of series A with porosity: 55.3% and pore size: 224 $\mu$m. (b) Sample of series B with porosity: 53.6% and pore size: 410 $\mu$m

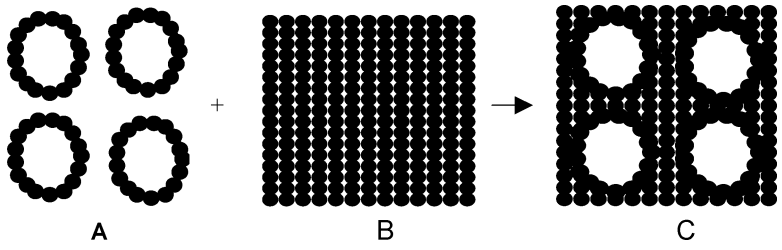


**Fig. 3** Schematic combination of pores in porous bodies is shown as (C). (A) Urea powders (white) are always covered by titanium powders (dark), which forms composed cells named Cell A. (B) A stack of titanium powders is named Cell B

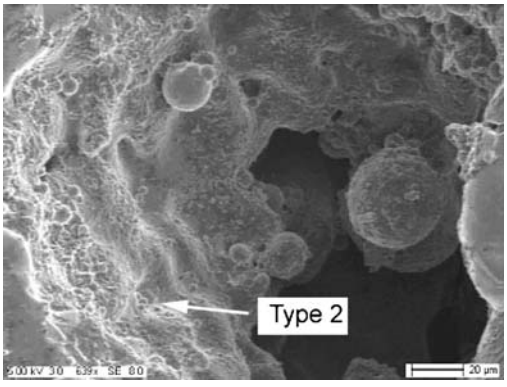


**Fig. 4** Picture of microstructures in one pore of 'Type 1' is taken by SEM. Its rough wall is composed by pores of 'Type 2'

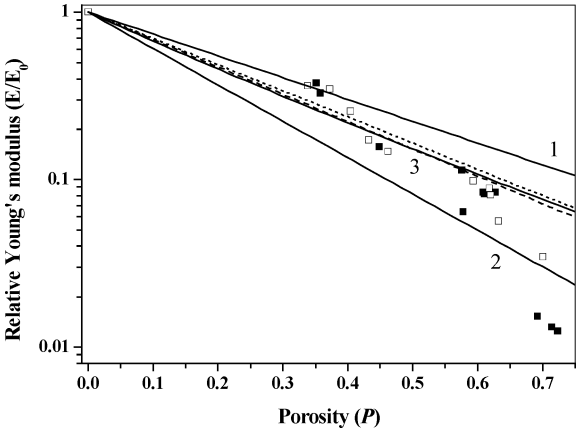


**Fig. 5** Semi-log plots of data of relative Young's modulus ($E/E_0$) versus the porosity ($P$) of samples of series A (■) and series B (□). The value of 'b' is based on Eq. (2): $E/E_0 = exp\ (-bP)$. Solid line 1 (—) with $b = 3$, for samples with Cell A, i.e. spherical pores in cubic stacking; solid line 2 (—) with $b = 5$, for samples with Cell B, i.e. solid spheres in cubic stacking. Solid line 3 (—) is given by the parallel model. Both break lines are given by ten times iterates of the Levenberg-Marquardt method. (a) For samples of series A, 'b' in dash line (- - - -) is $3.763 \pm 0.232$. (b) For samples of series B, 'b' in dot line (. . . .) is: $3.602 \pm 0.182$

urea powders are distorted in all directions. Titanium powders are also a little distorted and the contact area of them increases to form stable necks. After the urea powder decomposed during heat treatment, Cell A without collapse is considered as a hollow cell whose size is changed by the size of urea powder. As shown in Fig. 4, the bigger pore generated from decomposing of urea powder is named 'type 1' and interconnected with other ones. On its pore wall there are pores named 'Type 2', which are originated from irregular stacking of titanium powders just as Cell B in Fig. 3(B) and dispersed or grown larger in the followed procedure of compacting and sintering. Irregular pores of both type 1 and type 2 will become round driven by the decreased free energy of the whole system [22] during heat treatment.

### 3.2. Relation between Young's modulus and porosity

While changing the weight ratio of titanium to urea powders, the porosity of samples is controlled in a wide range (33–70%) as shown in Fig. 5. From the semi-log plots of Young's modulus ($E$) versus the porosity ($P$), it was found that with increased porosity the value of $E$ firstly decreases linearly, then decreases rapidly and goes to zero at certain porosity.

For modeling the elastic properties of porous solids [4, 14, 23–26], there is one approach based on pertinent cross-sectional geometries named the Minimum Solid Area (MSA) method [27–33]. It assumes the minimum solid area normal to the stress should dominate the transmission of stress (i.e. strain, fracture toughness or energy, or strength) through a body and be related to the mechanical properties of porous bodies [32, 33]. In this method, porous bodies are idealized reasonably for packing solid spheres or bubbles in some arrays, e.g. cubic, orthorhombic, rhombic and so on. The elastic properties of porous bodies are derived using these idealized structures to calculate actual solid cross-sectional areas. Minimum solid areas for stacked particles are the bond areas between them; for stacked bubbles are the minimal web cross-sectional areas between pores. The tendency of relative Young's modulus varied with porosity ($P$) of samples can be shown by

$$\frac{E}{E_0} = e^{-bP} \tag{2}$$

where $E_0$ is the Young's modulus of bulk metal (for titanium, $E_0$ is 105 Gpa [1]) and the value '$b$' is varied with the idealized packing geometry in bodies [31–33].

The basic characteristic of the MSA model [33] is that on a plot of the log of the property versus the value of $P$, the minimum solid area (and hence the pertinent property

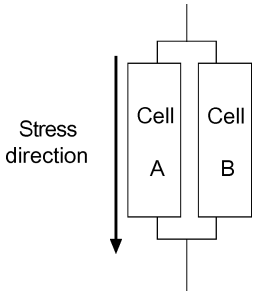


**Fig. 6** Samples with Cell A and Cell B in a parallel model are stacking along the stress direction

value of interest) decreases first, approximately, though not exactly, along straight lines on the semi-log plot. Beyond this approximately linear region the property of interest starts decreasing more rapidly, then nearly precipitously, going to zero at a critical porosity ($P_C$). It is obviously that the semi-log plots of Young's modulus versus the porosity as shown in Fig. 5 have these features of the MSA model. Here the value of '$b$' and '$P_C$' will be used for predicting the trends of Young's modulus varied with the porosity in the following parts.

Because of the insignificant dependence of elastic properties on microstructure stress concentration [30, 34, 35], the apporximation of the geometry of porous titanium can be justified to a nominal special-pores system. Powders in either Cell A or Cell B shown in Fig. 3 are idealized to be of spherical shapes. After the urea powder is removed during heat-treatment, Cell A is treated as a hollow sphere. Spheres in both samples with Cell A and those with Cell B are supposed to be arranged in a cubic array. The value '$b$' in Eq. (2) for samples with Cell A, i.e. with spherical pores in cubic stacking and for samples with Cell B, i.e. with solid spheres in cubic stacking, is 3 and 5; the relation based on Eq. (2) is shown as solid line 1 and solid line 2 in Fig. 5, respectively. Almost all experimental data lie between these two lines. Modeling porous titanium with two types of pores, samples with Cell A and Cell B are stacked together parallel to the applied stress as shown in Fig. 6 and flexural stresses will be distributed onto the minimum solid areas of two parts in a certain proportion. For the dynamic Young's modulus, this combination is named a parallel model giving the formula [32] as

$$\frac{E}{E_0} = V_A E_A + V_B E_B \tag{3}$$

where $V_A$, $V_B$, $E_A$ and $E_B$ are the volume fraction, the relative elastic property of samples with Cell A and with Cell B, respectively. The solid line 3 in Fig. 5 is given by the parallel model based on Eq. (3) with $V_A$ of 50% and $V_B$ of 50%. The break line given by ten times iterates of the Levenberg-Marquardt method shows the actual tendency of experimental data. It is obviously that solid line 3 and break line have shown almost the same tendency for Young's modulus varied with the porosity. But the fluctuations in the value of Young's modulus are observed. It is believed that the fluctuations are caused by an inhomogeneous material distribution. Porous titanium is a statistical system and therefore a certain spatial variation in porosity cannot be avoided. This inhomogenous distribution in porous bodies give rise to changes in the porosity of any part of the sample, and correspondingly, lead to a change in the values of $V_A$ and $V_B$ of Eq. (3), thus, the fluctuations of Young's modulus against porosity are observed.

In a further way to investigate the curve fitting by Eq. (2) with different values of '$b$', the deviations ($DE$) between the experiment data and calculated values, the mean deviation ($MD$) and the standard deviation ($SD$) are considered and given as:

$$DE = E_{\text{exp}} - E_{\text{cal}}, \tag{4}$$

$$ME = \frac{1}{n}\sum_{n}\sqrt{(DE)^2}, \tag{5}$$

$$SD = \frac{1}{n}\sum_{n}\sqrt{(DE - ME)^2}, \tag{6}$$

where $E_{\text{exp}}$ is the experimental relative elastic property and $E_{\text{cal}}$ is the calculated data. The values of $MD$ and $SD$ for samples with different pore structures, i.e. with the different value of 'b' are given in Table 1. It can be concluded that the parallel model can give a good prediction of dynamic Young's modulus of porous titanium with two types of pores.

It has long been known that while some types of porosity in bodies inherently can extend to $P$ values of nearly 1 (the ultimate limit), many types of porosity cannot exist in solid bodies above lower values of $P$. For idealized samples

**Table 1** Mean deviation and standard deviation for samples with different pore structures, i.e. with different values of 'b'

| | $b$ | 3 | 5 | Given by the parallel model | Given by Levenberg-Marquardt method |
|---|---|---|---|---|---|
| Samples of series A | $MD$, ($\times 10^{-2}$) | 7.14 | 5.36 | 4.23 | 3.91 |
| | $SD$, ($\times 10^{-2}$) | 3.91 | 6.36 | 3.43 | 3.28 |
| Samples of series B | $MD$, ($\times 10^{-2}$) | 6.02 | 6.77 | 3.74 | 3.76 |
| | SD, ($\times 10^{-2}$) | 3.84 | 6.71 | 3.30 | 2.42 |

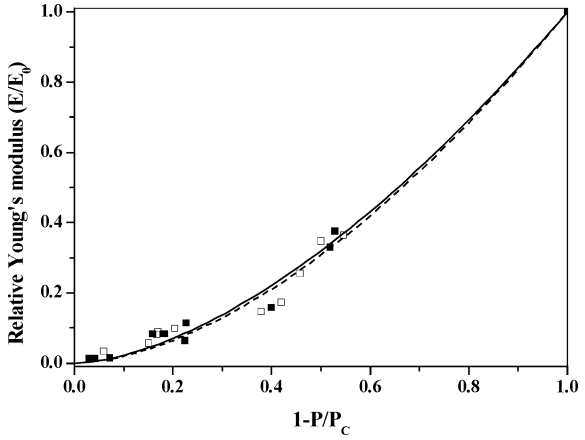


**Fig. 7** Linear plots are for relative Young's modulus versus the value of $1 - P/P_C$, where $P/P_C$ is named as normalized porosity and $P_C$ is the percolation limit. For samples of series A (■) and series B (□), $P_C$ is $0.745 \pm 0.0142$ and $0.744 \pm 0.0240$, respectively. The experiment data is fit by the power law model, $E/E_0 = (1 - P/P_C)^n$: for samples of series A and series B shown by solid Line (—) with $n = 1.646 \pm 0.0613$ and dash Line (- - - -) with $n = 1.700 \pm 0.0692$, respectively

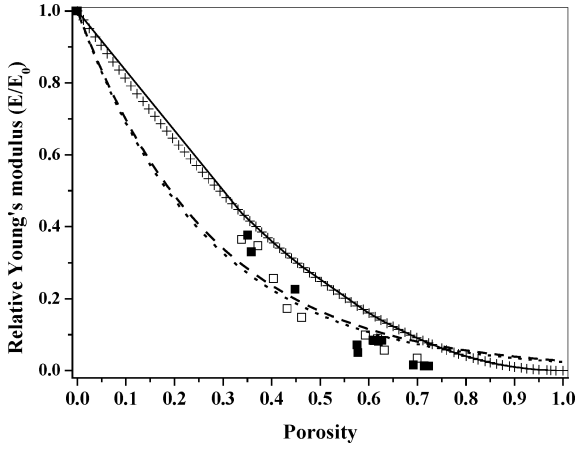


**Fig. 8** The relation between relative Young's modulus and porosity of samples of series A (■) and series B (□) are fit by all formulas. The solid line (—) and scatter points (+) are showing the formula given by the Gibson and Ashby's model and CSM model, respectively. The parallel model was shown by dot line (. . . .) with $b = 3.763 \pm 0.232$ and dash line (- - - -) with $b = 3.602 \pm 0.182$ for samples of series A and series B, respectively

with Cell A, i.e. with spherical pores in cubic stacking, the percolation limit, $P_C$, is calculated as 1, above which the minimum web areas between pores goes to zero; for idealized samples with Cell B, i.e. with solid spheres in cubic stacking, it is calculated as 0.524, above which the bond area between pores goes to zero. In our work, the average value of $P_C$ is got by extrapolating data trends as shown in Fig. 5. For samples of series A and B, it is determined as $0.745 \pm 0.0142$ and $0.744 \pm 0.0240$, respectively. It is found that the percolation limit for porous titanium with two types of pores is almost equal to the value for samples with the combination of two idealized porosities, which is determined by Eq. (3) of the parallel model. Then, using the normalized porosity [36], $P/P_C$, the relative Young's modulus is reconsidered by the power law model of the form: $E/E_0 = (1 - P/P_C)^n$ as shown in Fig. 7. The average fitting value $n$ is $1.646 \pm 0.0613$ and $1.700 \pm 0.0692$ for samples of series A and B, respectively. It is concluded that the power law model is valid in the full $P$ range because all plots have gone through the two diagonal end points of 0.0 (below this value the minimum solid area of porous bodies become zero) and 1.0 (at this value there are no pores in metal bodies).

On the basis of the MSA method, Gibson and Ashby [37] also gave a detailed theory on solid foam. An formula for predicting Young's Modulus of samples with open-porosity is given as:

$$\frac{E}{E_0} = k(1 - P)^2 \tag{7}$$

where $k$ is a constant and taken as '1'. Eq. (7) is valid on the limit of low relative density (<0.15).

formula as followed:

$$\frac{E}{E_0} = \frac{(1 - P)^2}{1 + \beta_E P} \tag{8}$$

where $\beta_E$ is calculated as $\frac{(1-5\mu_0)(3\mu_0-1)}{2(7-5\mu_0)}$ and the Poisson's ratio ($\mu_0$) of bulk titanium is 0.34 [1].

Data fitting by Eq. (3), (7) and (8) is performed in Fig. 8. In the low range of porosity (<65%), the relation between apparent [4] or dynamic Young's modulus of porous titanium and the porosity is poorly fit by Eq. (7). This relation can be well predicted by Eq. (3) given by the parallel model. For higher porosity Eq. (7) and (8) is closer with the tendency.

### 3.3. Relation between Young's modulus and pore size

Changing the size of urea powders, samples with different pore size are prepared and shown in Fig. 2. As shown in Fig. 6, after ten times alternative of the Levenberg-Marquardt method, the simulated value '$b$' is $3.763 \pm 0.232$ and $3.602 \pm 0.182$ for samples of series A and B, respectively. As shown in Fig. 7, the percolation limit, $P_C$ is $0.745 \pm 0.0142$ and $0.744 \pm 0.0240$ for samples of series A and series B, respectively. Thus, it can be concluded that the significant distinctions between them are not found.

## 4. Conclusions

In summary, porous titanium with controlled porosity and pore size is prepared in the procedure of powder metallurgy. The samples with open-porosity in the range of 33%–70%

and pore size from 200 $\mu$m to 500 $\mu$m are suitable for attachment and proliferation of the new ingrown bone tissues [41]. The dynamic Young's modulus of porous titanium with different morphology is measured by the EMAR method. The range of Young's modulus (1-40GPa) covers the range of cortical bones' modulus (10-40 Gpa) [1]. Porous titanium with appropriate elastic properties, i.e. similar with replaced bones', will reduce the effect of stress shielding and be preferred for bone substitute.

**Acknowledgements** This work was supported by the Natural Science Foundation of China under grant No. 10374089.

## References

1. M. Long and H.J. Rack, Biomaterials **19**, 1621 (1998).
2. J.J. Jacobs, D.R. Sumner, and J.O. Galante, Orthop. Clin. North Am. **24**, 583 (1993).
3. S. Thelen, F. Barthelat, and L.C. Brinson, J. Biomed. Mater. Res. **A69**, 601 (2004).
4. C.E. Wen, Y. Yamada, K. Shimojima, Y. Chino, T. Asahina, and M. Mabuchi, J. Mater. Sci-Mater. M **13**, 397 (2002).
5. I.H. Oh, N. Nomura, N. Masahashi, and S. Hanada, Scripta Mater. **49**, 1197 (2003).
6. D.C. Dunand, Adv. Eng. Mater. **6**, 369 (2004).
7. A.G. Kostornov and S.M. Agayan, Sov. Powder Met. Metal. Cer. **29**, 804 (1990).
8. M. Bram, C. Stiller, H.P. Buchkremer, D. Stöver, and H. Baur, Adv. Eng. Mater. **2**, 196 (2000).
9. C.E. Wen, M. Mabuchi, Y. Yamada, K. Shimojima, Y. Chino, and T. Asahina, Scripta Mater. **45**, 1147 (2001).
10. C.E. Wen, Y. Yamada, K. Shimojima, Y. Chino, H. Hosokawa, and M. Mabuchi, J. Mater. Res. **17**, 2633 (2002).
11. G. Rausch and J. Banhart, in Handbook of Cellular Metals: Production, Processing, Applications edited by H.P. Degischer and B. Kristz (Willey Press, 2002), p. 21.
12. D. Pohl, Powder Metall Int. **1**, 26 (1969).
13. G. Straffelini, V. Fontanari, and A. Molinari, Mater. Sci. Eng. **360A**, 197 (1999).
14. M. Eudier, Powder Metall. **9**, 278 (1962).
15. R. Haynes and J.T. Egediege, Powder Metall. **32**, 47 (1989).
16. T.J. Griffiths and A. Ghanizadeh, Powder Metall. **29**, 129 (1986).
17. J.R. Moon, Powder Metall **32**, 132 (1989).
18. H. Ogi, J. Acoust. Soc. Am. **106**, 660 (1999).
19. A.S. Nowick and B.S. Berry, Anelastic Relaxation in Crystalline Solids (Academic Press, New York and London, 1972), p. 626.
20. A. Wolfenden, M.R. Harmouche, G.V. Blessing, Y.T. Chen, P. Terranova, V. Dayal, V.K. Kinra, J.W. Lemmens, R.R. Phillips, J.S. Smith, P. Mahmoodi, and R.J. Wann, J. Test Eval. **17**, 2 (1989).
21. S. Spinner and W.E. Tefft, Proceedings ASTM **61**, 1221 (1961).
22. F.V. Lenel, Powder metallurgy: principles and applications (Metal powder Industries Federation. Princeton, New Jersey, 1980), p. 241.
23. K.K. Phani, J. Mater. Sci. **31**, 272 (1996).
24. T.E. Matikas, P. Karpur, and S. Shamasundar, J. Mater. Sci. **32**, 1099 (1997).
25. T. Ichitsubo, M. Tane, H. Ogi, M. Hirao, T. Ikeda, and H. Nakajima, Acta Mater. **50**, 4105 (2002).
26. D.T. Queheillalt, D.J. Sypeck, and N.G.H. Wadley, Mater. Sci. Eng. **A323**, 138 (2002).
27. R.M. Spriggs, J. Am. Ceram Soc. **44**, 628 (1961).
28. R.W. Rice, J. Am. Ceram Soc. **59**, 536 (1976).
29. R.W. Rice, J. Am. Ceram Soc. **76**, 1801 (1993).
30. R.W. Rice, J. Mater. Sci. **28**, 2187 (1993).
31. R.W. Rice, Key. Eng. Mater. **115**, 1 (1996).
32. R.W. Rice, J. Mater. Sci. **31**, 102 (1996).
33. R.W. Rice, J. Mater. Sci. **31**, 1509 (1996).
34. R.W. Rice, J. Mater. Sci. **32**, 4731 (1997).
35. A.K. Mukhopadhyay and K.K. Phani, J. Mater. Sci. **33**, 69 (1998).
36. R.W. Rice, J. Mater. Sci. **40**, 983 (2005).
37. L.J. Gibson and M.F. Ashby, Cellular Solids: Structure and Properties (2nd edn.). (Cambridge University Press, 1997), pp. 175–282.
38. N. Ramakrishnan and V.S. Arunachalam, J. Am. Ceram. Soc. **76**, 2745 (1993).
39. L.F. Nielson, Mater. Sci. Eng. **52**, 39 (1982).
40. L.F. Nielson, J. Am. Ceram. Soc. **67**, 93 (1983).
41. J.E. Lemons (ed.), Porous Implant, ASTM, STP **953**, 185 (1987).